

Neural Networks for cosmological model selection and feature importance using Cosmic Microwave Background data

I. Ocampo,^{a,1} G. Cañas-Herrera,^b S. Nesseris^a

^aInstituto de Física Teórica UAM-CSIC, Universidad Autónoma de Madrid, Cantoblanco, 28049 Madrid, Spain

^bESTEC - European Space Agency, Keplerlaan 1, 2201 AZ Noordwijk, The Netherlands

E-mail: indira.ocampo@csic.es, Guadalupe.CanasHerrera@esa.int, savvas.nesseris@csic.es

Abstract. The measurements of the temperature and polarisation anisotropies of the Cosmic Microwave Background (CMB) by the ESA Planck mission have strongly supported the current concordance model of cosmology. However, the latest cosmological data release from ESA Planck mission still has a powerful potential to test new data science algorithms and inference techniques. In this paper, we use advanced Machine Learning (ML) algorithms, such as Neural Networks (NNs), to discern among different underlying cosmological models at the angular power spectra level, using both temperature and polarisation Planck 18 data. We test two different models beyond Λ CDM: a modified gravity model: the Hu-Sawicki model, and an alternative inflationary model: a feature-template in the primordial power spectrum. Furthermore, we also implemented an interpretability method based on SHAP values to evaluate the learning process and identify the most relevant elements that drive our architecture to certain outcomes. We find that our NN is able to distinguish between different angular power spectra successfully for both alternative models and Λ CDM. We conclude by explaining how archival scientific data has still a strong potential to test novel data science algorithms that are interesting for the next generation of cosmological experiments.

Contents

1	Introduction	1
2	Methodology	4
2.1	Theoretical predictions in beyond- Λ CDM models	6
2.1.1	Deviations from general relativity	6
2.1.2	Search for primordial features	6
2.2	Machine Learning pipeline using Neural Networks	8
2.2.1	Simulated datasets	8
2.2.2	Neural Network architecture	9
3	Results and discussion	12
3.1	Deviations from general relativity: Hu-Sawicki model	12
3.2	Search for primordial features: linearly-spaced template	13
3.3	ML interpretability and assessment tests	14
4	Conclusions	17

1 Introduction

The Cosmic Microwave Background (CMB) is a remnant radiation from after the Hot Big Bang, and its detailed observations are crucial to the era of precision cosmology [1]. The CMB consists of photons that were emitted around 380 000 years after the Big Bang, at a time when the Universe had cooled enough for neutral atoms to form (at a redshift about $z \sim 1100$). Prior to this period, the Universe was a hot and dense plasma, where photons were continuously scattering with electrons. For this reason, the CMB represented the photon-electron last scattering surface of the moment when both types of particles were coupled to each other. It contains important information about the underlying cosmological model that best explains the latest observations of our Universe [2, 3].

The Planck satellite, launched by the European Space Agency in 2009 [4–6], is a reference in modern cosmology thanks to its exquisite measurements of the temperature and polarisation anisotropies of the CMB [7]. The CMB radiation is highly isotropic with a temperature of approximately 2.7 K, as first studied by the COBE satellite [8], and it is predicted to present small anisotropies showing under and overdensed regions in the primordial universe. In fact, the NASA WMAP satellite [9, 10], which followed on COBE, and the ESA Planck satellite [11], measured the temperature and polarization anisotropies to an exceptionally precise level. The discovery of these anisotropies presented in the CMB introduced a revolutionary approach to understand how our Universe works, and how the initial seeds that populated the very early Universe evolved to form the current Large-Scale Structure (LSS) we observed in the Universe. In general, we study the underlying cosmological model by comparing observable predictions, such as the angular power spectrum decomposition of the temperature and polarisation anisotropies, against real CMB data. These observations enabled to impose stringent constraints on the underlying physical model, called the standard cosmological concordance model, or simply, the Λ CDM (with the best fit values in table [Table 1](#)). This model assumes that the Universe’s accelerated expansion can be explained in

Parameter	Description	Planck alone
$\Omega_b h^2$	Baryon density parameter	0.022383
$\Omega_c h^2$	Cold dark matter density parameter	0.12011
$100\theta_{\text{MC}}$	Angular size of the sound horizon	1.040909
τ	Optical depth to reionization	0.0543
$\ln(10^{10} A_s)$	Amplitude of the primordial scalar perturbations	3.0448
n_s	Scalar spectral index	0.96605
H_0 [km s ⁻¹ Mpc ⁻¹]	Hubble constant	67.32
Ω_Λ	Dark energy density parameter	0.6842
Ω_m	Matter density parameter	0.3158
σ_8	Matter fluctuation amplitude on 8 h^{-1} Mpc scale	0.8120

Table 1: The Λ CDM best fit 6 cosmological parameters from *Planck* CMB temperature and polarization power spectra. The table is divided in the main sampled and derived parameters, like H_0 or σ_8 .

terms of a Cosmological constant in the dynamic equations (Λ , popularly associated to Dark Energy), that the main energy density component is Cold Dark Matter (CDM), and that the primordial density perturbations in the early Universe were almost Gaussianly-distributed, compatible with the predictions of the vanilla single-field inflation model. On top, CMB data has given powerful insights on alternative inflationary models [7], the nature of dark matter and dark energy [5, 12, 13], and the homogeneity of our Universe [14].

Despite its success in explaining observational phenomena, the Λ CDM model has faced some challenges and is currently the focus of intense research. There is a lack of understanding of its two main components (Dark Matter and Dark Energy) and also, the precision level we have reached in parameter extraction, could imply potential tensions in our current understanding of the Universe [15–17], which include the cosmic dipoles problem [18], the age of the Universe [19], the lithium problem [20], etc¹. Perhaps the most debated problem is the so-called Hubble *tension*, which arises during the first release of cosmological parameters from the Planck Collaboration [4], from the discrepancy of the Hubble constant found by CMB early Universe observations: $H_0 = 67.4 \pm 0.5$ km s⁻¹Mpc⁻¹ and the value obtained by late-time surveys like SH0ES: $H_0 = 73.04 \pm 1.04$ km s⁻¹Mpc⁻¹ [22, 23].

Understanding the late-time Universe’s acceleration and its relation with the Hubble tension is a current hot discussion topic in cosmology [24, 25]. The discrepancies on its value may arise from observational systematic effects, statistical fluctuations, or new physics beyond the Λ CDM model. This is one of the reasons that, despite the Λ CDM model being a very good statistical fit that explains most of the observational phenomena, there is still interest in discovering few extension models that can explain the unresolved cosmological late-time accelerated expansion but yet recover the Λ CDM expansion history and pass the Solar System tests [26, 27]. Many viable Modified Gravity (MG) theories feature “screening mechanisms” that cause deviations from General Relativity (GR) to switch off on small scales, leaving them with significantly different predictions from GR only over cosmological distances [28].

Within the MG framework, the $f(R)$ family of theories is an interesting alternative beyond Λ CDM, since it is the most natural extension performed in the Einstein-Hilbert action, at the level of the Ricci scalar, i.e. $R \rightarrow f(R) \simeq R + mR^2$ [29]. Some studies on

¹For an extensive review, see [21].

cosmological constraints on these theories can be found in [30–32]. A popular viable model within these theories that is in agreement with the Λ CDM expansion history and that passes the Solar System tests is the Hu-Sawicki (HS) model [33]. In this case, the corresponding expansion of $f(R)$ takes the form,

$$f(R) = -6\Omega_{\text{DE},0}\frac{H_0^2}{c^2} + |f_{R0}|\frac{\bar{R}_0^2}{R} + \dots, \quad (1.1)$$

where $f_{R0} = \text{d}f(R)/\text{d}R|_{z=0}$ and for values of $|f_{R0}| \ll 1$ the Λ CDM expansion history is well recovered. In this work, we choose the value of $|f_{R0}| = 10^{-6}$, so that we are still in agreement with observations while we perform a comparison of models [34].

Furthermore, the Λ CDM model also fails to give an explanation about the nature of the origin of the Universe. The anisotropies of the CMB indicates that the primordial density perturbations that populated the very early Universe should have been almost Gaussianly distributed, explaining the observed homogeneity and isotropy of the cosmos. Inflation is widely regarded as the mechanism responsible for the origin of these primordial density perturbations and, by construction, solves the horizon and flatness problems. This exponentially rapid expansion phase took place fractions of a second after the Big Bang provides a solid framework for the generation of primordial density fluctuations that raised the current LSS. These fluctuations are imprinted on the primordial power spectrum (PPS), which describes the distribution of these density perturbations across different scales. In the simplest inflationary model, vanilla canonical single-field inflation, this power spectrum is usually defined as:

$$P_{\mathcal{R},0}(k) = \frac{2\pi^2}{k^3}\mathcal{P}_{\mathcal{R},0}(k) = A_s \left(\frac{k}{k_\star}\right)^{n_s-1}, \quad (1.2)$$

where n_s and A_s are the spectral index and the amplitude of the comoving curvature perturbations, respectively, and $k_\star = 0.05 \text{ Mpc}^{-1}$ is the pivot scale.

In this sense, Equation 2.6 is compatible with the assumptions of the Λ CDM, setting a phenomenological parametrisation of an *almost*-scale invariant power spectrum. However, it lacks an intrinsic mechanism to explore further inflationary scenarios or further alternatives, making the study of deviations from this power-law a hot topic in cosmology [35].

Over the past years, an explosion of data has significantly contributed to numerous studies for testing deviations from Λ CDM. These works have been carried out with data from late time Universe, like BOSS [36], DES [37], KiDS [38] and early Universe with the characterization of CMB fluctuations with WMAP [10], Planck [6] and ACT [39]. In the future, it is expected that the most precise constraints of the cosmological model parameters will come from stage IV surveys such as the ESA *Euclid* mission [40–42], LSST [43] and DESI [44], which are promising to constrain extensions beyond the Λ CDM model.

This explosion of data collection, beyond allowing an increase in quantity and quality, will pose questions on how to efficiently analyse the data and how to adapt computational pipelines. This is one of the main reasons why Machine Learning (ML) has become more popular in cosmology in the past years. The primary benefits of ML techniques lay in its ability to uncover patterns, insights, and knowledge from large datasets without explicit instructions, and to adapt and enhance its performance independently. Therefore, ML methods can fully unlock the potential of multi-probe cosmology by effectively improving systematic effects and optimally integrating information from various surveys [45]. It facilitates the detection and classification of cosmological sources as well as the extraction of information from images [46, 47]. ML methods have also been introduced to cosmological simulations for robust predictions

(see [48]). Additionally, some work has been done in the context of cosmological parameter inference [49–51] and for testing models beyond Λ CDM in the context of galaxy clustering [34] and weak lensing [52]. Furthermore, some studies using CMB data and ML were performed, for example for lensing reconstruction [53] and deep learning of CMB radiation temperature [54].

While the official operations of the ESA Planck mission came to an end, after showing the capacity of the CMB temperature and polarisation anisotropies in constraining the underlying cosmological model, it can still be leveraged to provide stringent tests for theories of fundamental physics beyond the Λ CDM. In the context of the late-time Universe we can test MG models related to dark energy, like the Hu-Sawicki model, and in the case of the early Universe we can use the data it to search for deviations in the primordial power spectrum power-law (the so-called features). Therefore, the aim of this work is to test both cases using Planck 18 CMB angular power spectrum, to perform ML-based model selection. For this, we train and test a Neural Network with first, HS simulated data vs Λ CDM simulated data and second, feature models simulated data vs Λ CDM, both cases taking into account the Planck 18 data uncertainties.

The layout of our paper is the following. In [section 2](#), we introduce the two beyond- Λ CDM cases we want to test, the Hu-Sawicki model and the linear feature model in the primordial power spectrum ([subsection 2.1](#)), and we explain how we simulated our training data and created our neural network architecture ([subsection 2.2](#)). In [section 3](#), we show the results of the analysis and comment on the main characteristics found: in [subsection 3.1](#) and [subsection 3.2](#) we discuss the results from the analysis of the Hu-Sawicki model and the primordial feature template respectively, and, finally, we discuss the interpretability of our machine learning pipeline in [subsection 3.3](#). Finally, in [section 4](#), we summarise our findings, explain the main lessons learnt and draw possible future work to further exploit our Machine Learning pipeline.

2 Methodology

The focus of this study is the development and performance evaluation of a robust data analysis pipeline for machine learning-based model selection, in order to study two cases, (1) deviations from general relativity within the framework of the Hu-Sawicki model and (2) searching for primordial features in the primordial power spectrum. To achieve this, we implemented an architecture based on Neural Networks to work with Planck 18 data at the level of the CMB angular power spectra C_ℓ . The angular power spectra is given by [55, 56]

$$C_\ell^{XY} = \frac{2}{\pi} \int k^2 dk P(k) \Delta_\ell^X(k) \Delta_\ell^Y(k), \quad (2.1)$$

where XY stands for the TT, TE and EE polarisation patterns, $P_{\mathcal{R}}(k)$ is the power-law primordial spectrum given by [Equation 2.6](#), and $\Delta_\ell^X(k)$ is the transfer function that is related to the evolution of primordial density fluctuations from their primordial state to the time of recombination and beyond, and ℓ is the multipole moment [2, 56]. We can also rewrite the angular power spectra in the common \mathcal{D}^{XY} definition:

$$\mathcal{D}_\ell^{XY} = \frac{\ell(\ell+1)C_\ell^{XY}}{2\pi}. \quad (2.2)$$

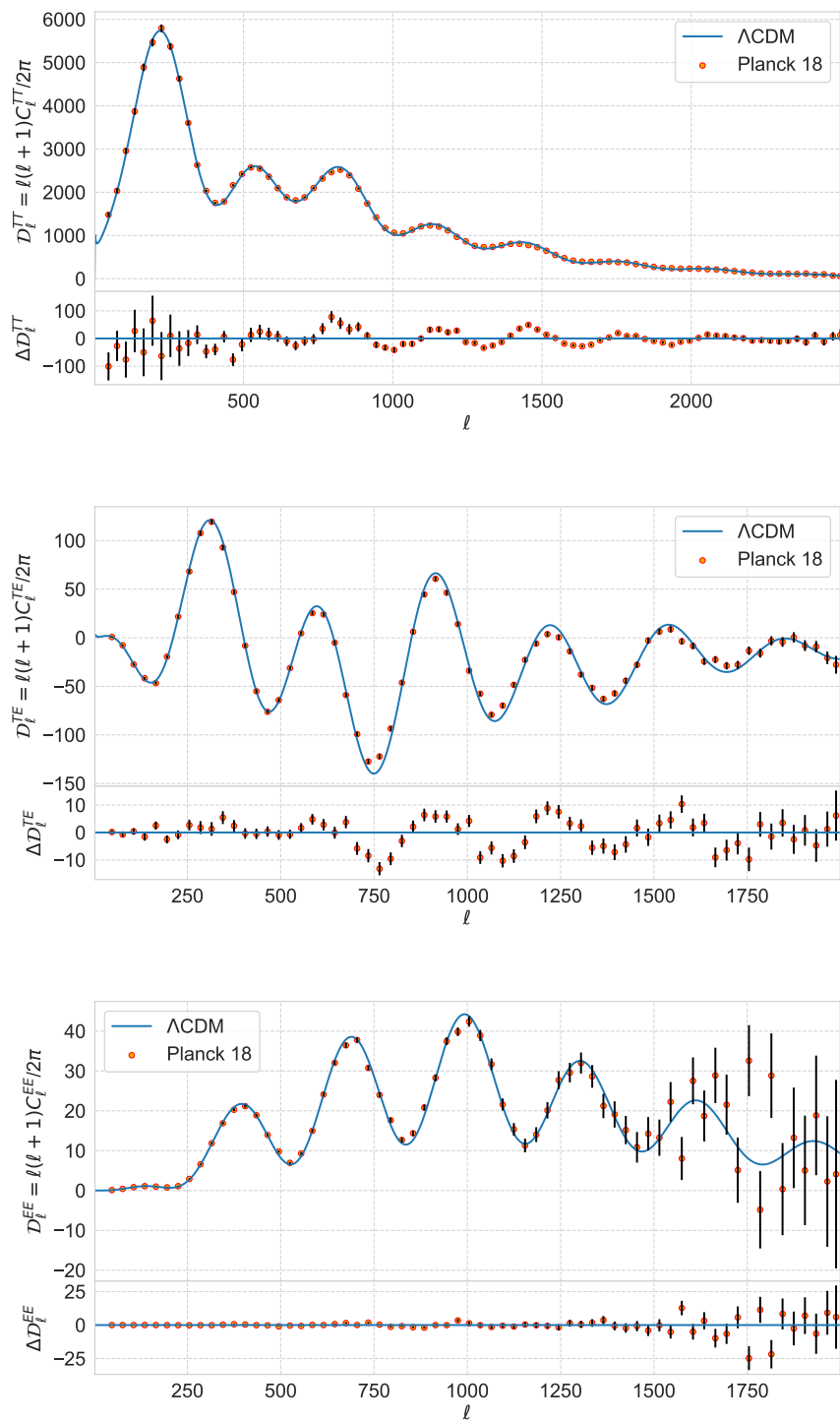


Figure 1: Top panels: CMB angular power spectra Planck 18 binned temperature TT, polarisation EE, and cross-correlations TE anisotropies (orange dots, with error bars), jointly with the best theory prediction from Λ CDM (solid blue line), calculated with CLASS. Bottom panels: difference with respect to the best fit for all the different components.

The transfer function $\Delta_{\mathcal{X}\ell}(k)$ is usually calculated using so-called Boltzmann solvers CAMB [57] or CLASS [58]. An important aspect of Equation 2.1 is that any late-time Universe or modified gravity model is reflected in the transfer function, subsequently affecting the angular power spectra, whereas any deviation originating from the early Universe physics impacts the power-law primordial power spectrum $P_{\mathcal{R}}(k)$, which also induces changes in the angular angular power spectra. This interplay makes it an ideal framework for testing both scenarios.

We are interested in studying the statistical properties of the CMB anisotropies, characterized by the temperature (TT mode), polarization (EE mode) and cross (TE) angular power spectra, since the position and amplitude of the peaks and dips of these spectra are sensitive to the assumed underlying cosmological model. See, for example, Figure 1, which shows the Planck 18 angular power spectrum binned data² compared to the best fit prediction of the Λ CDM model. For every computation of the Λ CDM baseline model, we chose the fiducial cosmological parameters according to Planck 18 cosmological results [6], as noted in Table 1, and the software CLASS.

2.1 Theoretical predictions in beyond- Λ CDM models

2.1.1 Deviations from general relativity

The scenario to test for deviations from GR that we will stick to is the HS $f(R)$ model, having an effect on the transfer function that at the same time has an impact on the angular power spectrum Equation 2.1 [59]. To see this, we consider a modification to the Einstein-Hilbert action of the form [33]:

$$S = \int d^4x \sqrt{-g} \left[\frac{1}{2\kappa} f(R) + \mathcal{L}_m \right], \quad (2.3)$$

where R is the Ricci scalar, \mathcal{L}_m is the matter Lagrangian and $\kappa = 8\pi G_N$ is a constant (with G_N being the Newton's constant). By varying the action and taking some considerations, like the sub-horizon and quasi-static approximations, we get to the following second order differential equation [60]:

$$\ddot{\delta} + 2H\dot{\delta} - 4\pi G_{\text{eff}} \rho \delta = 0, \quad (2.4)$$

where the dot represents the derivative with respect to the cosmic time t and,

$$G_{\text{eff}} = \frac{G_N}{F} \frac{1 + 4\frac{k^2}{a^2} \frac{F'}{F}}{1 + 3\frac{k^2}{a^2} \frac{F'}{F}}. \quad (2.5)$$

is the effective gravitational constant that accounts for the effect of modified gravity [60, 61]. Here $F(R) \equiv f'(R)$, the prime denotes derivative with respect to R , and a is the scale factor. Therefore, in this context, the only part affected by $f(R)$ is the transfer function. See [62] for a reference and [63–65] for current constraints on this model.

2.1.2 Search for primordial features

All cosmological observations so far align with the assumption of adiabatic, Gaussian, and nearly scale-invariant initial conditions. These results strongly support a specific inflationary scenario known as slow-roll inflation. This pattern is broadly accepted as matching the predictions of the simplest inflationary single-field canonical model [66, 67]. However, since

²The data can be found at the Planck Legacy Archive at <http://pla.esac.esa.int/pla>.

our observations only capture perturbations, deducing the background that produced them reveals that various underlying theories can lead to the same set of cosmological observables. If there are any features in the primordial power spectrum (deviations from the nearly scale-invariant power spectrum), they would provide a distinctive and revealing insight into the fundamental theory behind the mechanism that created these initial fluctuations [35]. Primordial features, $\Delta P_{\mathcal{R}}/P_{\mathcal{R},0}$, are parametrised as small deviations from the power-law primordial power spectrum introduced in Equation 2.6 as:

$$P_{\mathcal{R}}(k) = P_{\mathcal{R},0}(k) \left[1 + \frac{\Delta P_{\mathcal{R}}}{P_{\mathcal{R},0}}(k) \right], \quad (2.6)$$

where $P_{\mathcal{R},0}$ is given by Equation 2.6. There are several theories that predict different SHAPes for features (localised, linear or logarithmic spaced ones). In this paper we study a toy-model feature template with oscillations linearly spaced in Fourier space with a constant amplitude, superimposed on the power-law (see Figure 2):

$$\frac{\Delta P_{\mathcal{R}}}{P_{\mathcal{R},0}} = A_{\text{lin}} \sin \left(\omega_{\text{lin}} \frac{k}{k_{\star}} + \phi \right), \quad (2.7)$$

where A_{lin} is the amplitude of the feature, ϕ is some arbitrary phase and ω_{lin} is the frequency of oscillations. The fiducial values of the parameters that define the linear oscillations Θ_{lin} are given by [68],

$$\Theta_{\text{lin}} = \{A_{\text{lin}} = 0.01, \omega_{\text{lin}} = 10, \phi_{\text{lin}} = 0\}. \quad (2.8)$$

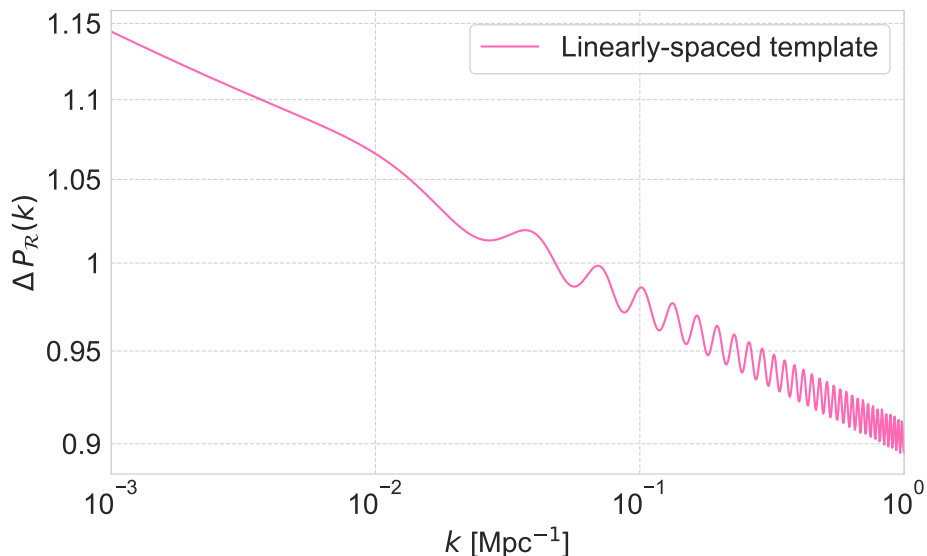


Figure 2: Linearly-spaced primordial feature $\Delta P_{\mathcal{R}}$ on the power spectrum of curvature perturbations, given the fiducial values at Equation 2.8, as a function of scale, in logarithmic space.

The discovery of any additional inflationary signals hidden in the data could significantly change our understanding of the early stages of the Universe. While, several feature templates have been tested against Planck 18 data [7], developing an alternative pipeline to test features

could offer a way to test extensive photometric and spectroscopic surveys, which offer a complementary perspective on large-scale structures (LSS). This enhances the sensitivity to high-frequency signals and complements CMB measurements.

2.2 Machine Learning pipeline using Neural Networks

The Planck mission provided detailed measurements of the anisotropies of the CMB, allowing to perform cosmological inference on dark energy and modified gravity [5] and inflation [4] models, as well as putting the tightest constraints on cosmological parameters [6] by sampling the posterior distribution of the parameters of interest using Markov Chain Monte Carlo (MCMC) exploration of the likelihood. Instead, this work has the objective to test GR deviations from Λ CDM and search for primordial features leveraging the power of Neural Networks (NN). NNs are known to be a powerful tool consisting of many connected units known as neurons that produce a sequence of real-valued activations, and are widely used in classification tasks. Within these algorithms, deep neural networks are one of the most popular and are characterized for having fully connected (dense) layers, i.e. all possible connections layer-to-layer are present [69]. Deep NN can enhance the accuracy of model predictions and improve our understanding of the physical processes behind certain patterns. This is an important task in cosmology, since distinguishing between models could potentially lead to some insights into the nature of the evolution of the Universe, dark matter and dark energy, and could set a preliminary starting point for an exhaustive (classical) statistical analysis on a later time. The analysis pipeline and datasets are publicly available on GitHub³ and Zenodo⁴, respectively.

2.2.1 Simulated datasets

To train and test our NN, we simulated two types of datasets:⁵

- **Deviations from general relativity (Hu-Sawicki model):** We generated the dataset using MGCLASS⁶ [70], a modified version of the Boltzmann solver CLASS, within the framework of the HS model. We simulated 1000 samples (since the scalability of the code does not compensate the performance of the NN) for Λ CDM baseline model (see Table 1) varying Ω_{cdm} within the range [0.1, 0.15], and 1000 for the $f(R)$ model with grids of values $|f_{R0}| \in [10^{-6}, 5 \times 10^{-6}]$, for three components C_{ℓ}^{TT} , C_{ℓ}^{TE} and C_{ℓ}^{EE} . For this case, Planck 18 uncertainties derived from the corresponding covariance matrix, are subsequently incorporated into the data. Finally to study the point in which the NN performance breaks down for this section, we also generated data for $|f_{R0}|$ for different ranges spanning $[10^{-4}, 5 \times 10^{-4}]$, $[10^{-6}, 5 \times 10^{-6}]$, $[10^{-7}, 5 \times 10^{-7}]$ and $[10^{-8}, 5 \times 10^{-8}]$.
- **Search for primordial features (linearly-spaced template):** We generated a synthetic dataset using a modified version of the Boltzmann solver code CLASS [58] by introducing the target linearly-spaced feature in the primordial power spectrum (Equation 2.7). We used the Planck best fit cosmological parameters Table 1 to generate 500 samples (once again, because the scalability of the code does not compensate the performance of the NN), of the angular power spectrum for Λ CDM varying $\Omega_{\text{cdm}} \in [0.05, 0.15]$,

³https://github.com/Indira0campo/CMB_ML_based_model_selection.git

⁴Primordial feature template (10.5281/zenodo.13829664), and Hu-Sawicki (10.5281/zenodo.13828966)

⁵Note that we use the term *datasets* to refer to the synthetic self-generated data used to train the neural network (using Planck 18 uncertainties), and it should not be mistaken with the real Planck 18 data.

⁶<https://gitlab.com/zizgitlab/mgclass--ii/s>

and 500 for the linearly-spaced primordial feature, varying Ω_{cdm} in the same range and $A_{\text{lin}} \in [10^{-2}, 5 \times 10^{-2}]$. We followed this procedure for each of the three components: C_ℓ^{TT} , C_ℓ^{TE} and C_ℓ^{EE} and added the uncertainties from the covariance matrix set out of the Planck errors. We also aimed to test the point in which the NN performance breaks down, so we also generated data for A_{lin} for different ranges between $[10^{-3}, 5 \times 10^{-3}]$, $[10^{-4}, 5 \times 10^{-4}]$, $[10^{-5}, 5 \times 10^{-5}]$ and $[10^{-6}, 5 \times 10^{-6}]$.

2.2.2 Neural Network architecture

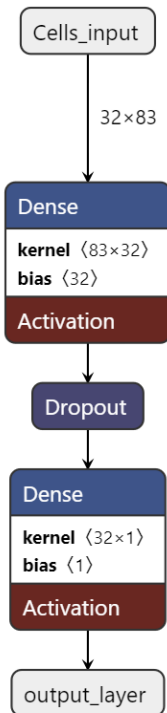


Figure 3: NN architecture for the TT case with 83 neurons in the input layer (that accounts for the 83 data points of each C_ℓ^{TT} realization). We set the batch size to the default 32 value, followed by the implementation of a fully connected layer of 32 neurons, a dropout layer and an output layer with one neuron.

Different architectures can influence how effectively a NN can capture underlying patterns and features within the data. In this paper, we chose deep neural networks, because of their potential in classification tasks. We developed 4 different deep NN: one for each CMB angular power spectra case (TT, TE, EE), and a final one for the joint case (TT + TE + EE). A generalized scheme of the implemented NN's architecture is shown in [Figure 3](#), where the units (neurons) in the input layer depended on the number of data points of each case: for C_ℓ^{TT} – 83 units, for C_ℓ^{TE} – 66 units, for C_ℓ^{EE} – 66 units and the last one for the combined analysis $C_\ell^{TT} + C_\ell^{TE} + C_\ell^{EE}$ – 215 units. The units correspond to the number of data points present in Planck 18 binned data.

The efficiency of training a deep NN heavily relies on the quality of the input data. Therefore, it is essential to assess, clean, and process the data to maximize the NN's ability

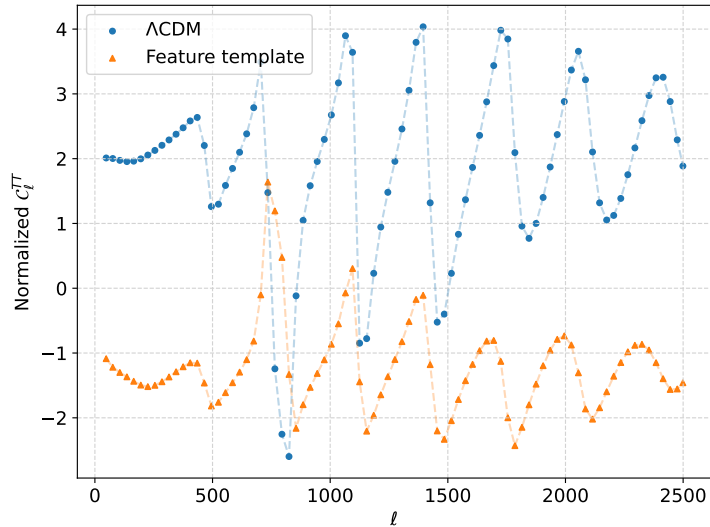


Figure 4: Illustration of how the Z-score normalization for the C_ℓ^{TT} CMB power spectrum maximize the differences between Λ CDM and extension models (in this case, the linearly-spaced feature template as in Equation 2.7). The Z-score normalization not only re-scales the mean of the C_ℓ^{TT} but also highlights the difference in phase for the C_ℓ^{TT} values as a function of ℓ .

to learn key features. Common approaches for achieving this are statistical normalization techniques. In this case, we applied the so-called Z-score normalization for the data pre-processing, which consists on measuring how many standard deviations σ a data point is from the mean of the dataset μ , and use this reference setup to effectively re-scale the whole dataset so that $\mu = 0$ and $\sigma = 1$ [71]. To exemplify this in our analysis, we show the impact of using Z-score normalization in one of our datasets; in particular, on the C_ℓ^{TT} component for the feature model case (see Figure 4). The differences on C_ℓ^{TT} after normalization between Λ CDM and the linearly-spaced feature template are more evident, allowing the deep NN to easily identify possible features for further classification and identification. Similar results are found for the HS model. We performed the same Z-score normalization for the pre-processing of all 8 architectures (4 for the HS model and 4 for the primordial feature model). Furthermore, we have assessed the impact of using the Z-score normalization on the \mathcal{D}_ℓ (see Equation 2.2) instead of C_ℓ to train the NN, not finding significant differences in the output and therefore, re-assuring the stability of the NN architecture.

After completing the data pre-processing steps, we divided the 1500 data realizations (with 50% corresponding to Λ CDM and 50% to either HS or primordial features, depending on the scenario) into two sets: 70% for training and 30% for testing. We set the batch size to 32, and incorporated a hidden dense layer with 32 units with a ReLU activation function [72]. We included a dropout layer (with a dropout rate of 0.2) as regularisation technique to prevent over-fitting [73]. Finally, we added the last dense layer with one unit and a sigmoid activation function that enhances the classification score for the model: 0 – Λ CDM and 1 – HS or primordial feature. The models were compiled with an Adam optimizer (learning_rate = 0.0002), a binary cross entropy loss function, and trained over a 1000 epochs.

See Figure 3 for a schematic view of one of the NN's architecture.

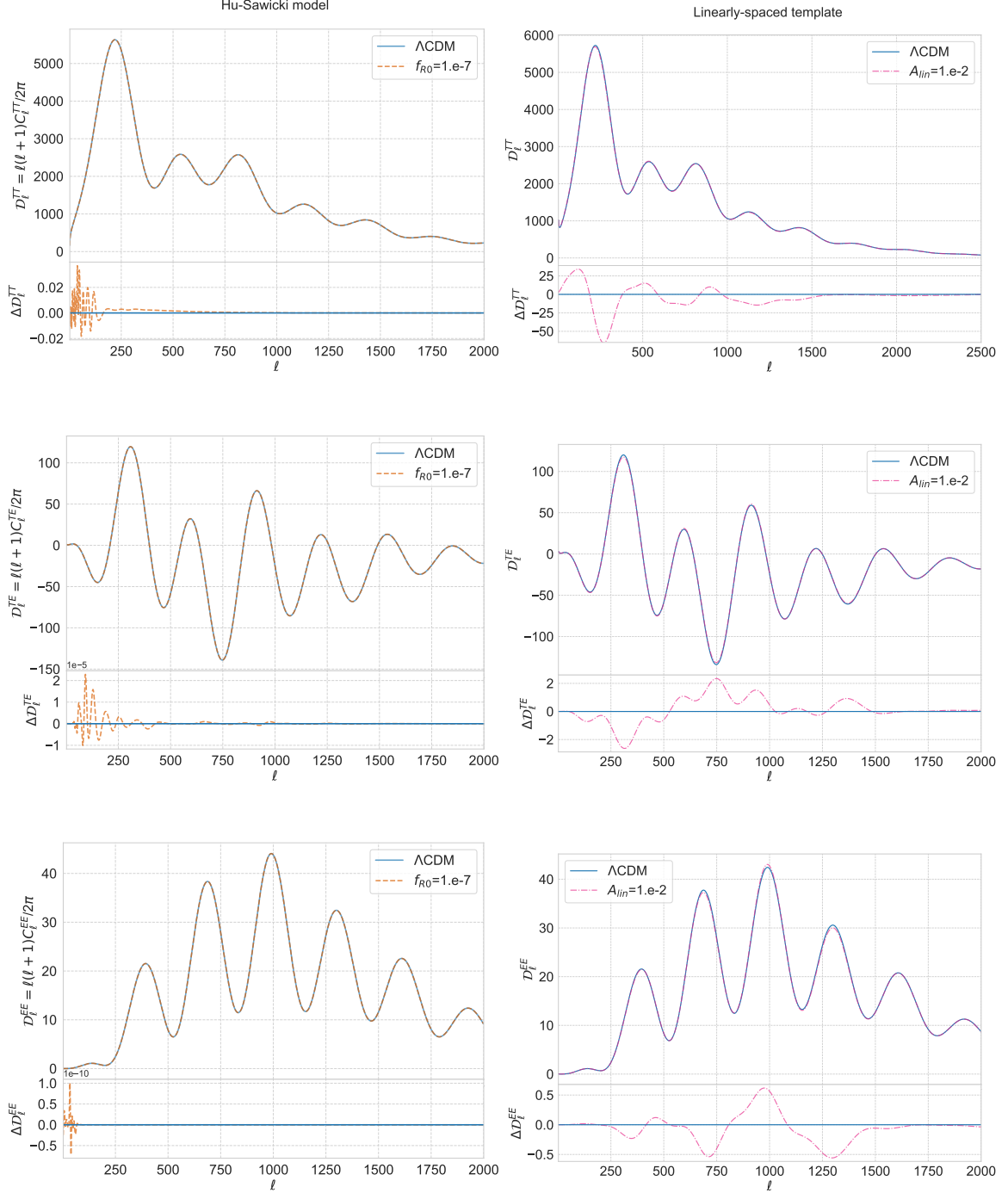


Figure 5: Left: f_{R0} effect on the TT, TE and EE components. Right: Feature template on the primordial power spectrum, this is reflected on the effect of the A_{lin} parameter size on the TT, TE and EE components.

3 Results and discussion

In this section, we present the main results obtained with our pipeline and the outcome of the learning assessment with ML interpretability. The classification performance of our NN’s architecture is available in [Table 2](#) for the three components C_ℓ^{TT} , C_ℓ^{TE} , C_ℓ^{EE} and its combination $C_\ell^{TT} + C_\ell^{TE} + C_\ell^{EE}$, for both the two cases under study (deviations from general relativity and features in the primordial power spectrum). We used ranges of parameters that encompassed the fiducial values of both models as $A_{\text{lin}} = 10^{-2}$ and $|f_{R0}| = 10^{-6}$ (see [Figure 5](#)). From these results, we can see that the NNs perform better in detecting the alternative initial conditions in the context of the early Universe physics than the deviations from GR in the late-time Universe.

CMB components	Hu-Sawicki model		linearly-spaced feature	
	Correct	Wrong	Correct	Wrong
C_ℓ^{TT}	0.93	0.07	1	0
C_ℓ^{TE}	0.47	0.53	1	0
C_ℓ^{EE}	0.48	0.52	1	0
$C_\ell^{TT} + C_\ell^{TE} + C_\ell^{EE}$	0.88	0.12	1	0

Table 2: Performance of Neural Networks classification when trained and tested on each component of the temperature and polarization angular Power Spectrum, and its combined analysis. Two models were studied: for the early Universe case, a linearly-spaced template to search for primordial features in the primordial power spectrum (with a range of values of $A_{\text{lin}} \in [10^{-2}, 5 \times 10^{-2}]$), and for the late-time Universe, the Hu-Sawicki model to test for deviations from Λ CDM (with a range of values of $|f_{R0}| \in [10^{-6}, 5 \times 10^{-6}]$).

3.1 Deviations from general relativity: Hu-Sawicki model

In the context of MG, the NN performance in detecting C_ℓ^{TT} coming from Λ CDM or HS is 0.93 (see [Table 2](#)), compared to the cases of the other components C_ℓ^{TE} and C_ℓ^{EE} , where the performance drops to 0.47 and 0.48. When studying the case in which we combined all the data, we concluded that the NN is mostly learning to differentiate between models mainly from the temperature angular power spectrum component.

To understand this, we illustrate in [Figure 5](#) the effect of f_{R0} on the C_ℓ components of the CMB, where only the C_ℓ^{TT} one is affected by the changes in this parameter. This is why the performance of the NN to classify between Λ CDM and HS is clearly better in the temperature angular power spectrum than the other two cases: C_ℓ^{TE} and C_ℓ^{EE} do not show any deviations in HS with respect to Λ CDM. We also aimed to study the point (if any) in which the NNs performance breaks down or changes, so we generated datasets for different ranges of f_{R0} , and then compared the performance on each of them, and also the combined case $C_\ell^{TT} + C_\ell^{TE} + C_\ell^{EE}$. This information is available in [Figure 6](#), where we can notice that for the C_ℓ^{TT} case, the performance breaks down for values of $|f_{R0}| = 10^{-7}$, and for the other two modes, the NN cannot differentiate between models regardless of the value of this parameter. This value has proven to be still in agreement with current surveys (see, for example [\[74\]](#)), while the Λ CDM model is recovered with $|f_{R0}| = 0$. In fact, the NN was able to *learn* a feature of the HS model: the HS model only shows deviations on the C_ℓ^{TT} component (see [\[75\]](#) where they verify that this is indeed the case by comparing Boltzmann

solvers). This blind test strengthens the robustness of our pipeline, as the NN could not classify the data realization as neither Λ CDM nor HS using C_ℓ^{TE} and/or C_ℓ^{EE} .

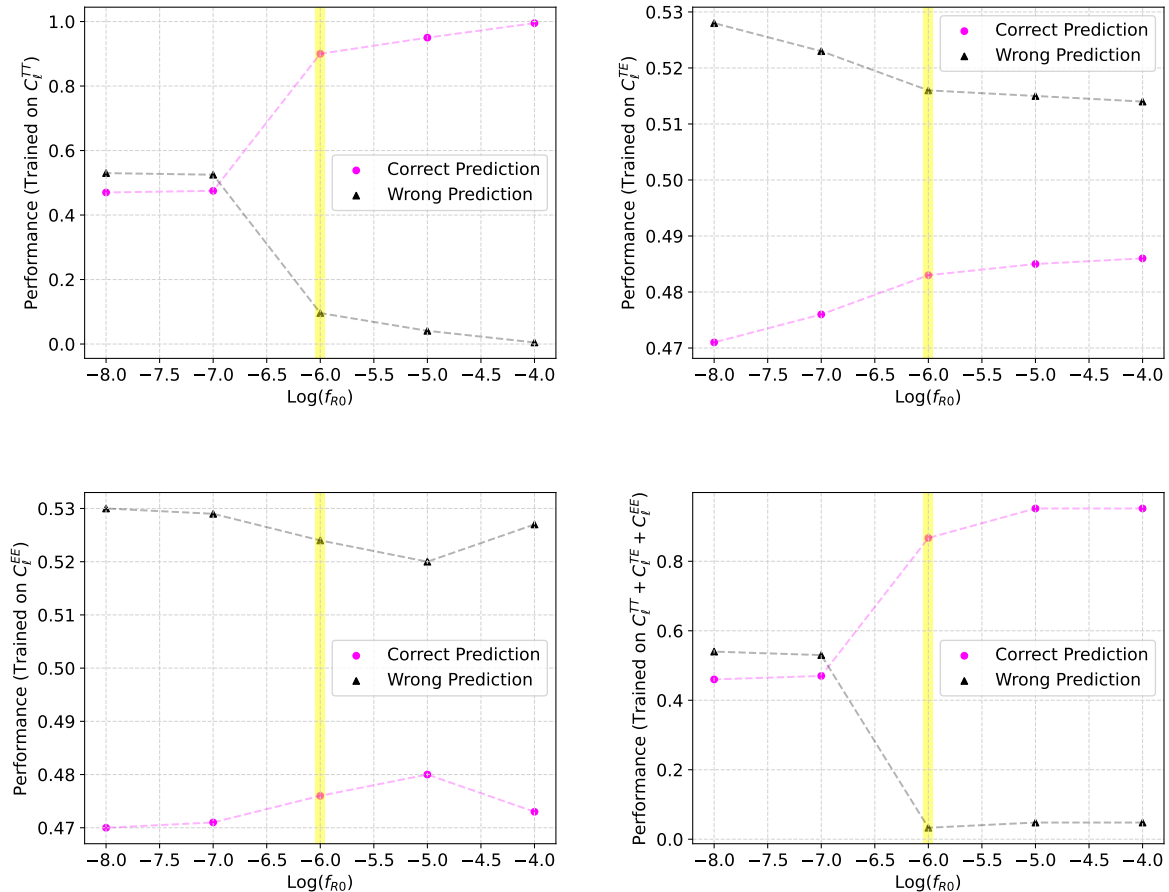


Figure 6: Semi-log plot of f_{R0} values vs architecture performance for the components (up) C_ℓ^{TT} , C_ℓ^{TE} (bottom) C_ℓ^{EE} , joint analysis: $C_\ell^{TT} + C_\ell^{TE} + C_\ell^{EE}$. The yellow region corresponds to the fiducial value of $|f_{R0}| = 10^{-6}$.

3.2 Search for primordial features: linearly-spaced template

With respect to the case for features in the primordial power spectrum, defined as linearly-spaced, the NN is able to differentiate between models in all three angular power spectra, C_ℓ^{TT} , C_ℓ^{TE} and, C_ℓ^{EE} , and also for the combined case. In Table 2, we notice that the performance is 1 for all the cases, which is sensible if we see the effect of A_{lin} on the modes in ?? for the fiducial value of $A_{\text{lin}} = 10^{-2}$, where clear deviations are shown with respect to the Λ CDM model. This is expected since primordial features in the power spectrum are expected to introduce changes on all CMB C_ℓ components, as given by Equation 2.1.

For completion, we also analyzed the point in which the NN's performance breaks down, and for all the cases there is similar value of $A_{\text{lin}} = 10^{-4}$, where the correct prediction decreases to 0.4 for C_ℓ^{TT} and C_ℓ^{TE} and to ≈ 0.6 for C_ℓ^{EE} and the combined case (see Figure 7). In general, the NN is able to discern between Λ CDM and the linearly-spaced feature model for

fiducial values of A_{lin} . This is a highlight of our pipeline, since the NN is able to classify well even when the differences between the models are very small.

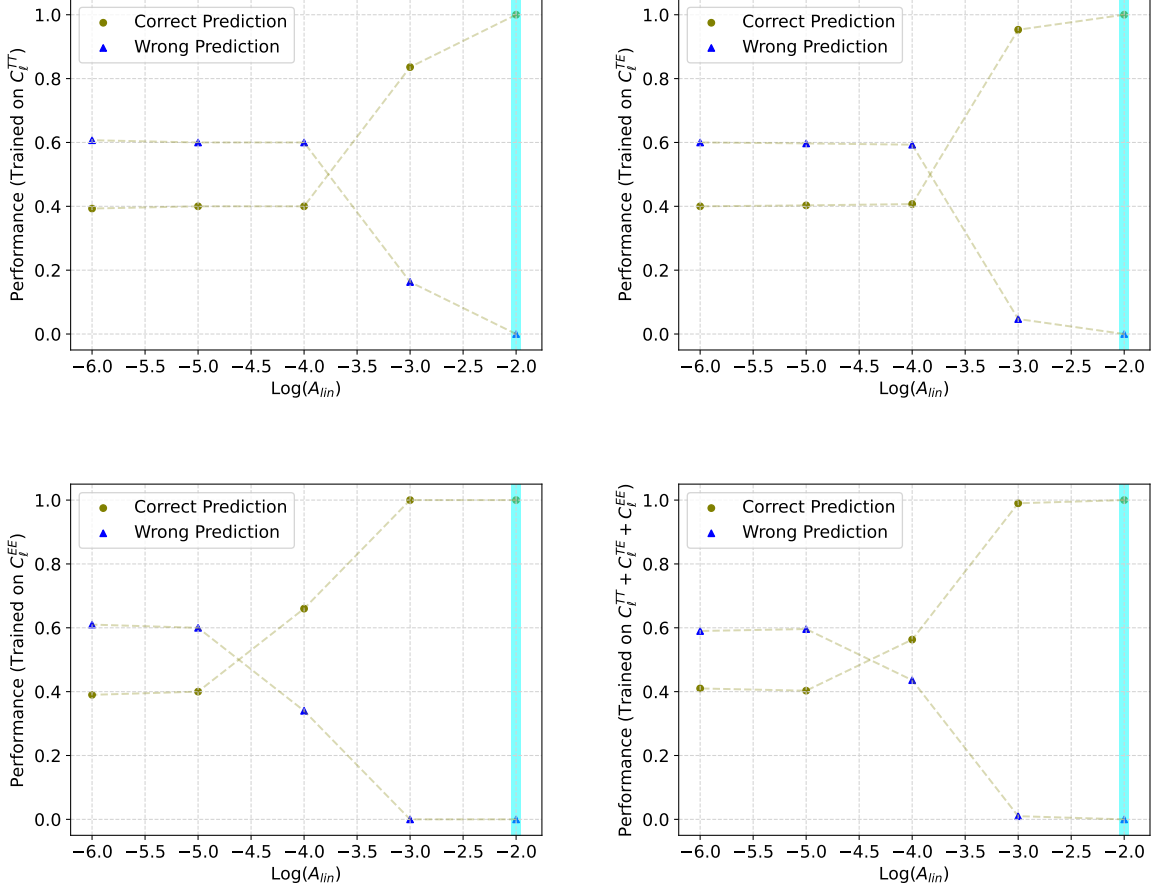


Figure 7: Semi-log plot of A_{lin} values vs architecture performance for the components (up) C_ℓ^{TT} , C_ℓ^{TE} (bottom) C_ℓ^{EE} , joint analysis: $C_\ell^{TT} + C_\ell^{TE} + C_\ell^{EE}$. The cyan region corresponds to the fiducial value of $A_{\text{lin}} = 10^{-2}$.

3.3 ML interpretability and assessment tests

Machine Learning (ML) interpretability has become essential in deep learning, as understanding how these ML techniques reach their conclusions is necessary for building trust in their application across various fields, particularly in analyzing complex datasets [76]. To assess how the NN learn, we focused our work on the interpretability tool known as SHAP (SHAPley Additive exPlanations)⁷. In general, ML interpretability follows two approaches: local and global explanations. Global explanations provide an overview of the learning’s process throughout the entire dataset, whereas the local method focuses on studying a region in the hyperparameter space. SHAP, which can be employed for both local and global explanations,

⁷<https://github.com/SHAP/SHAP.git>

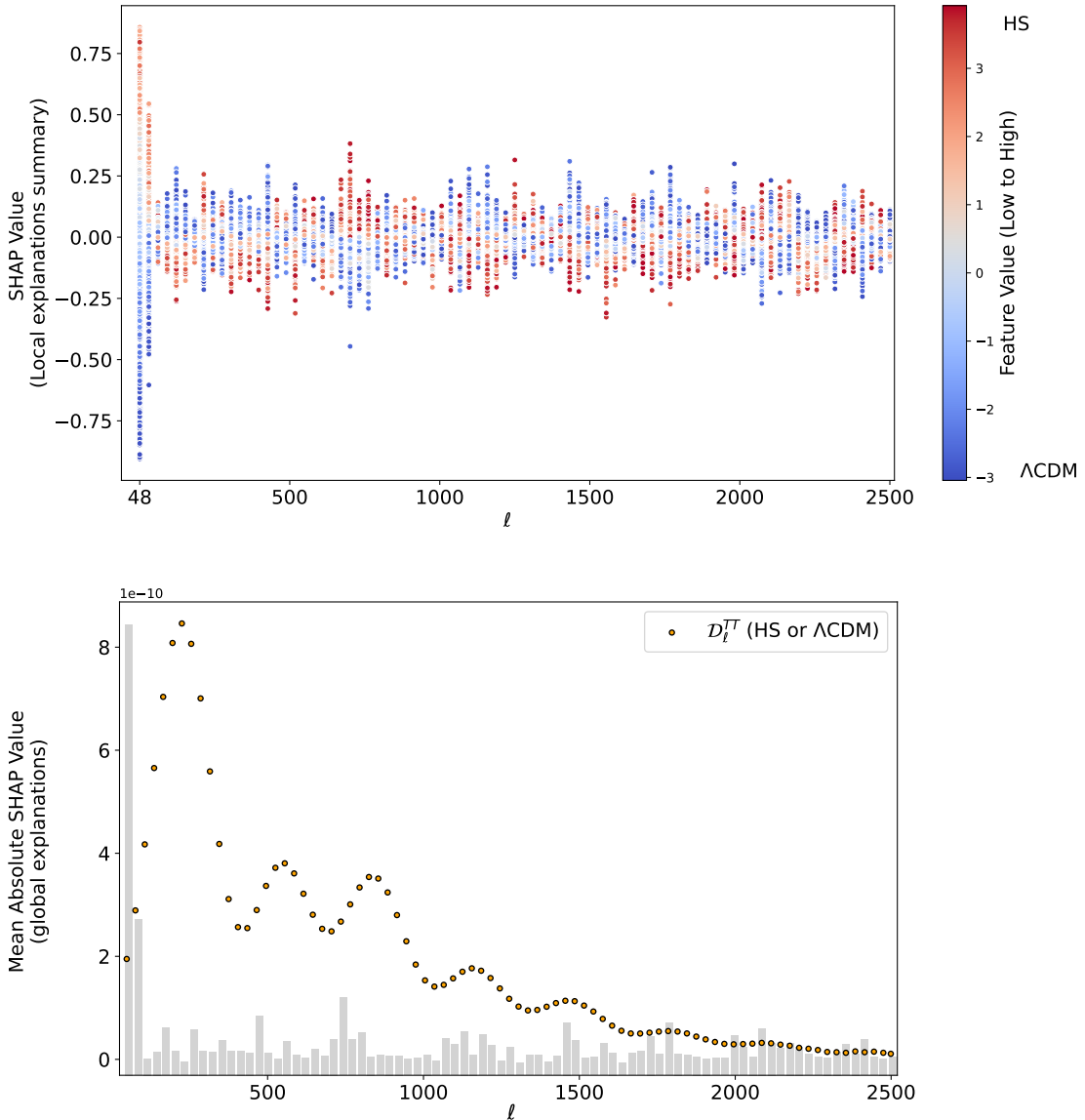


Figure 8: Machine Learning explanations for the Hu-Sawicki model. Top: local interpretability given by the SHAP values (high value, Hu-Sawicki and low value, Λ CDM). Bottom: global interpretability by the mean absolute SHAP values that corresponds to each C_ℓ^{TT} .

is a method for explaining the output of a NN architecture by attributing the contribution of each element to the final prediction, which is known as *feature importance*⁸.

SHAP is based on cooperative game theory, and helps to understand the most important input elements (or "players") by computing an adapted version of the so-called *Shapley values* [77]. It has a bottom-up approach: for the local explanations, it assesses the contribution of each input datapoint (in our case, the C_ℓ) to the prediction, by considering all possible combinations. In this context, Shapley values are calculated by introducing each element x

⁸Not to be confused with the feature template of the primordial power spectrum in extensions beyond single-field inflation; therefore in the body of the text of this work, we will refer to it as "element importance".

(one by one) into a conditional function of the model’s output

$$f_x(S) \approx E[f(x) | x_S], \quad (3.1)$$

which can be understood as the expected prediction given that only the elements in a subset S are known. The change in the model’s decision at each step is attributed to the newly introduced element. This process is then averaged across all possible element orderings to ensure a fair distribution of contributions. Hence, the SHAP values produces attributions $\phi_i(f, x)$ that matches the original model output $f(x)$ [77], given by,

$$\phi_i(f, x) = \sum_{m \in \mathcal{M}} \frac{1}{N!} [f_x(P_i^m \cup i) - f_x(P_i^m)], \quad (3.2)$$

where \mathcal{M} is the set of all feature orderings, P_i^m is the set of all elements that come before the i^{th} element in ordering m , and N is the number of input elements for the model. For a revision on this topic refer to [77, 78] and [79]. On the contrary, for the global interpretability approach, this method calculates the mean absolute SHAP values, giving an overall importance to each element for the model’s outcome.

In this work, SHAP is used for one of the first times as interpretability tool in cosmological model selection and interpretability [80, 81]. We employed SHAP for both, local and global interpretability assessments for the temperature angular power spectrum C_ℓ^{TT} for the two extension models. The analysis takes approximately 3 hours for each model. For the case of the modified gravity model, we can see the Hu-Sawicki NN explanations in Figure 8; the upper panel displays the local interpretability assessment with SHAP values that correspond to each \mathcal{D}_ℓ^{TT} . Higher values mean that their corresponding elements are more likely to contribute to a Hu-Sawicki outcome, and lower values to a Λ CDM one. In the lower panel, we see the global interpretability results with the mean absolute SHAP values, that correspond to each \mathcal{D}_ℓ^{TT} . The dots represent one randomly selected realization of the data (either belonging to the HS model or to Λ CDM). We observe how the first \mathcal{D}_ℓ^{TT} values are the critical one for the NN to learn the main elements to classify either Λ CDM or HS. This is expected as observed in Figure 5, where the main changes with respect to Λ CDM for the HS model take place at low multipole values.

Subsequently, in figure Figure 9, we show the explanations for the linearly-spaced primordial feature template model; as in the previous case, the upper panel displays the local interpretability part with SHAP values that correspond to each \mathcal{D}_ℓ^{TT} . In this case, higher values show that their corresponding elements are more likely to contribute to a feature-template model outcome, and lower values to a Λ CDM one. In the same way, the lower panel displays the global interpretability conclusions, with the mean absolute SHAP values, that correspond to each \mathcal{D}_ℓ^{TT} . Again, the dots represent one randomly selected realization of the data (either belonging to the feature-template model or to Λ CDM). In this case, both the local and global explanations trace properly the changes introduced in the \mathcal{D}_ℓ^{TT} due to the primordial feature template in Figure 2, identifying as critical those ℓ where the corresponding Planck 18 uncertainty is larger, and therefore, more likely to allow for deviations from the power-law primordial power spectrum. In summary, we notice that the NN are properly learning how to differentiate models based on the deviations displayed in the lower panels of Figure 5, because it seems that the peaks of the most important elements in both Figure 8 and Figure 9 coincide with these deviations. We also raise an interesting point by revisiting Table 2, where we conclude that NN perform better in differentiating the primordial feature template from

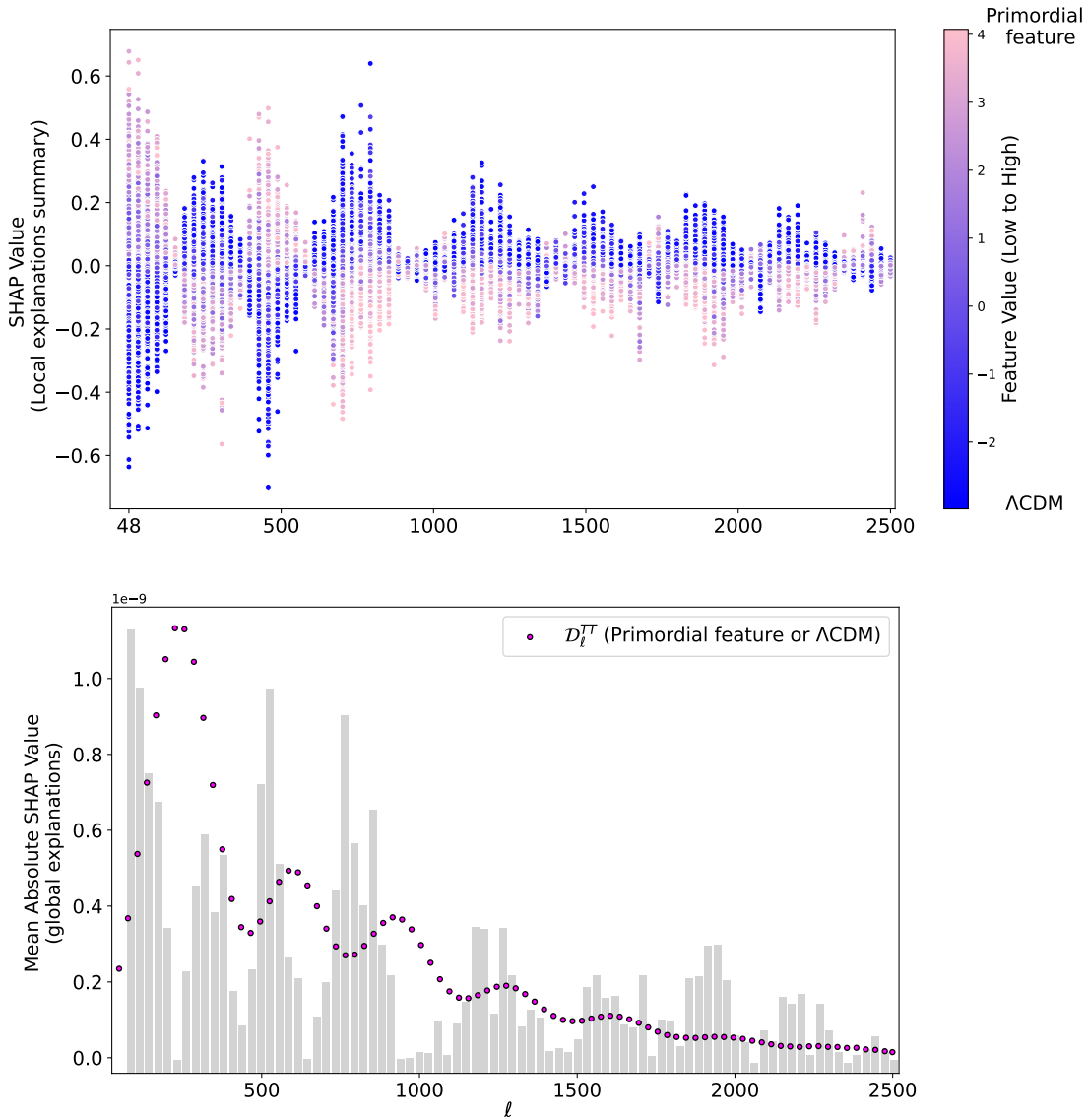


Figure 9: Machine Learning explanations for the linearly-spaced primordial feature model. Top: local interpretability given by the SHAP values (high values, primordial feature model and low ones, Λ CDM). Bottom: global interpretability by the mean absolute SHAP values that corresponds to each C_ℓ^{TT} .

Λ CDM than the case of Hu-Sawicki. In light of the SHAP values, this is expected because the primordial feature model displays more numerous important elements than those of the HS analysis, helping the NN identify the key-elements for classification.

4 Conclusions

In this work, we presented our Machine Learning pipeline designed for model selection using deep Neural Networks to classify two models beyond the Standard Cosmological Model. Our first focus was on late-time physics, specifically deviations from General Relativity within the

framework of the Hu-Sawicki $f(R)$ model. The second focus was on early universe hypotheses, particularly the search for linearly-spaced features in the primordial power spectrum. The architecture of our deep Neural Network pipeline has been optimized to maximize the learning of key features while minimizing over-fitting.

To train our pipeline, we generated Planck 2018-like data, including its specifications and uncertainties for the mentioned cases. We tested its ability to distinguish between data derived from the Hu-Sawicki model vs Λ CDM and the primordial feature model vs Λ CDM. Our pipeline comprises a total of eight Neural Networks: four dedicated to the three polarization modes and one that combines all of them for testing the linearly spaced primordial feature model, as well as four for evaluating the Hu-Sawicki model. Generally, the architectures remained consistent, with the primary variation being the number of neurons in the input layer, which corresponded to the number of binned Planck 2018 angular power spectrum data points.

The results demonstrate that our pipeline effectively learned the crucial elements necessary to classify the test dataset. Specifically, for the Hu-Sawicki datasets, the Neural Network achieved a correct prediction rate of 93% for the temperature power spectrum. However, for polarization and cross-data, the performance dropped to 0.47 and 0.48, respectively, aligning with theoretical expectations, as the Hu-Sawicki model does not exhibit differences compared to Λ CDM in the polarization CMB angular power spectra. This outcome indicates that our Neural Network accurately identified this insensitivity and successfully passed this sanity check. In the second scenario, we aimed to differentiate between the primordial linearly-spaced feature model and Λ CDM across temperature, polarization, and cross-data (as well as a combination of all three). Remarkably, the pipeline achieved a 100% correct prediction rate across all components, making this kind of ML pipelines highly useful in the community to assess the potential of a dataset to constrain features in the primordial power spectrum. In fact, this computationally cheaper approach can be applied before addressing a full Bayesian inference exercise to sample the probability posterior distributions of the features' parameters to actually discern the capacity to detect a possible primordial feature template.

To evaluate and understand how our pipeline is learning to classify amongst models, we implemented SHAP as an interpretability tool to extract meaningful insights about the main input elements that drive these Neural Networks to certain outcomes. The application of this particular interpretability tool is one of the first applications of SHAP to cosmological model selection. We confirmed that our architectures can differentiate between models by focusing on the elements of the angular power spectra that reflect the deviations between the proposed alternatives and Λ CDM, these key elements were identified prior to training. We conclude with highlighting our ML interpretability results, since feature importance is crucial for evaluating the learning process and deep learning algorithms do not always make decisions based on the features or elements we intend for them to learn.

Looking ahead to future work, we see potential for extending our work by applying the pipeline to classify models using CMB temperature and polarization maps, leveraging techniques like Convolutional Neural Networks or Graph Neural Networks. Additionally, we aim to apply the pipeline to other summary statistics from various cosmological observables, such as cosmic shear in Large-Scale Structure and photometric angular clustering power spectra.

Acknowledgments

We thank Dr. Stéphane Ilic for interesting discussions about the Planck 18 covariance matrices. IO thanks ESTEC/ESA for the warm hospitality during the execution of this project, and for support from the [ESA Archival Research Visitor Programme](#). IO thanks to Elena Donini for useful discussions during the ESA internship. IO and SN acknowledge support from the research project PID2021-123012NB-C43 and the Spanish Research Agency (Agencia Estatal de Investigación) through the Grant IFT Centro de Excelencia Severo Ochoa No CEX2020-001007-S, funded by MCIN/AEI/10.13039/501100011033. IO is also supported by the fellowship LCF/BQ/DI22/11940033 from “la Caixa” Foundation (ID 100010434). GCH acknowledges support through the ESA research fellowship programme.

References

- [1] RB Barreiro. An overview of the current status of cmb observations. *Highlights of Spanish Astrophysics V*, pages 93–102, 2010.
- [2] Daniel Baumann. Tasi lectures on inflation. *arXiv preprint arXiv:0907.5424*, 2009.
- [3] Wayne Hu. Lecture notes on cmb theory: From nucleosynthesis to recombination. *arXiv preprint arXiv:0802.3688*, 2008.
- [4] Planck Collaboration, PAR Ade, N Aghanim, C Armitage-Caplan, M Arnaud, M Ashdown, F Atrio-Barandela, J Aumont, C Baccigalupi, AJ Banday, et al. Planck 2013 results. xxii. constraints on inflation. *0004-6361*, 571:22, 2014.
- [5] Peter AR Ade, N Aghanim, M Arnaud, M Ashdown, J Aumont, C Baccigalupi, AJ Banday, RB Barreiro, Nicola Bartolo, E Battaner, et al. Planck 2015 results-xiv. dark energy and modified gravity. *Astronomy & Astrophysics*, 594:A14, 2016.
- [6] Nabila Aghanim, Yashar Akrami, Mark Ashdown, Jonathan Aumont, Carlo Baccigalupi, Mario Ballardini, Anthony J Banday, RB Barreiro, Nicola Bartolo, S Basak, et al. Planck 2018 results-vi. cosmological parameters. *Astronomy & Astrophysics*, 641:A6, 2020.
- [7] Yashar Akrami, Frederico Arroja, M Ashdown, J Aumont, Carlo Baccigalupi, M Ballardini, Anthony J Banday, RB Barreiro, Nicola Bartolo, S Basak, et al. Planck 2018 results-x. constraints on inflation. *Astronomy & Astrophysics*, 641:A10, 2020.
- [8] George F. Smoot, Charles L. Bennett, Alan Kogut, Edward L. Wright, Radek Stompor, et al. Structure in the coBE differential microwave radiometer first-year maps. *The Astrophysical Journal Letters*, 396:L1–L5, 1992.
- [9] David N Spergel, Licia Verde, Hiranya V Peiris, Eiichiro Komatsu, MR Nolta, Charles L Bennett, Mark Halpern, Gary Hinshaw, Norman Jarosik, Alan Kogut, et al. First-year wilkinson microwave anisotropy probe (wmap)* observations: determination of cosmological parameters. *The Astrophysical Journal Supplement Series*, 148(1):175, 2003.
- [10] Gary Hinshaw, D Larson, Eiichiro Komatsu, David N Spergel, CLaa Bennett, Joanna Dunkley, MR Nolta, M Halpern, RS Hill, N Odegard, et al. Nine-year wilkinson microwave anisotropy probe (wmap) observations: cosmological parameter results. *The Astrophysical Journal Supplement Series*, 208(2):19, 2013.
- [11] Peter AR Ade, Nabila Aghanim, Monique Arnaud, Mark Ashdown, J Aumont, C Baccigalupi, A Balbi, AJ Banday, RB Barreiro, JG Bartlett, et al. Planck early results. xviii. the power spectrum of cosmic infrared background anisotropies. *Astronomy & Astrophysics*, 536:A18, 2011.
- [12] Giacomo Galloni, Mario Ballardini, Nicola Bartolo, Alessandro Gruppuso, Luca Pagano, and Angelo Ricciardone. Unraveling the cmb lack-of-correlation anomaly with the cosmological

- gravitational wave background. *Journal of Cosmology and Astroparticle Physics*, 2023(10):013, 2023.
- [13] Douglas Scott, Dagoberto Contreras, Ali Narimani, and Yin-Zhe Ma. The information content of cosmic microwave background anisotropies. *Journal of Cosmology and Astroparticle Physics*, 2016(06):046, 2016.
- [14] Y. Akrami et al. Planck 2018 results. VII. Isotropy and Statistics of the CMB. *Astron. Astrophys.*, 641:A7, 2020.
- [15] William Giarè. Cmb anomalies and the hubble tension. *arXiv preprint arXiv:2305.16919*, 2023.
- [16] Jian-Ping Hu and Fa-Yin Wang. Hubble tension: the evidence of new physics. *Universe*, 9(2):94, 2023.
- [17] Elcio Abdalla, Guillermo Franco Abellán, Amin Aboubrahim, Adriano Agnello, Özgür Akarsu, Yashar Akrami, George Alestas, Daniel Aloni, Luca Amendola, Luis A Anchordoqui, et al. Cosmology intertwined: A review of the particle physics, astrophysics, and cosmology associated with the cosmological tensions and anomalies. *Journal of High Energy Astrophysics*, 34:49–211, 2022.
- [18] Chethan Krishnan, Ranjini Mondol, and MM Sheikh-Jabbari. Dipole cosmology: the copernican paradigm beyond flrw. *Journal of Cosmology and Astroparticle Physics*, 2023(07):020, 2023.
- [19] Licia Verde, Pavlos Protopapas, and Raul Jimenez. Planck and the local universe: Quantifying the tension. *Physics of the Dark Universe*, 2(3):166–175, 2013.
- [20] Brian D Fields. The primordial lithium problem. *Annual Review of Nuclear and Particle Science*, 61(1):47–68, 2011.
- [21] Leandros Perivolaropoulos and Foteini Skara. Hubble tension or a transition of the cepheid snia calibrator parameters? *Physical Review D*, 104(12):123511, 2021.
- [22] Adam G Riess, Wenlong Yuan, Lucas M Macri, Dan Scolnic, Dillon Brout, Stefano Casertano, David O Jones, Yukei Murakami, Gagandeep S Anand, Louise Breuval, et al. A comprehensive measurement of the local value of the hubble constant with 1 km s⁻¹ mpc⁻¹ uncertainty from the hubble space telescope and the sh0es team. *The Astrophysical journal letters*, 934(1):L7, 2022.
- [23] Pablo Lemos and Paul Shah. The cosmic microwave background and h_0 . *arXiv preprint arXiv:2307.13083*, 2023.
- [24] Dark Energy Survey Collaboration:, T Abbott, FB Abdalla, J Aleksić, S Allam, A Amara, D Bacon, E Balbinot, M Banerji, K Bechtol, et al. The dark energy survey: more than dark energy—an overview. *Monthly Notices of the Royal Astronomical Society*, 460(2):1270–1299, 2016.
- [25] Dark Energy Survey Collaboration: T Abbott et al. The dark energy survey. *International Journal of Modern Physics A*, 20(14):3121–3123, 2005.
- [26] Jai-chan Hwang and Hyerim Noh. $f(r)$ gravity theory and cmbr constraints. *Physics Letters B*, 506(1-2):13–19, 2001.
- [27] Pedro Bessa, Marcela Campista, and Armando Bernui. Observational constraints on starobinsky $f(r)$ cosmology from cosmic expansion and structure growth data. *The European Physical Journal C*, 82(6):506, 2022.
- [28] Alejandro Aviles, Jorge L Cervantes-Cota, and David F Mota. Screenings in modified gravity: a perturbative approach. *Astronomy & Astrophysics*, 622:A62, 2019.
- [29] Alexei A. Starobinsky. A new type of isotropic cosmological models without singularity. *Physics Letters B*, 91(1):99–102, 1980.

- [30] Spyros Basilakos, Savvas Nesseris, and Leandros Perivolaropoulos. Observational constraints on viable $f(r)$ parametrizations with geometrical and dynamical probes. *Physical Review D—Particles, Fields, Gravitation, and Cosmology*, 87(12):123529, 2013.
- [31] Soumya Jana and Subhendra Mohanty. Constraints on $f(r)$ theories of gravity from gw170817. *Physical Review D*, 99(4):044056, 2019.
- [32] Rafael C Nunes, Supriya Pan, Emmanuel N Saridakis, and Everton MC Abreu. New observational constraints on $f(r)$ gravity from cosmic chronometers. *Journal of Cosmology and Astroparticle Physics*, 2017(01):005, 2017.
- [33] Wayne Hu and Ignacy Sawicki. Models of $f(r)$ cosmic acceleration that evade solar system tests. *Physical Review D—Particles, Fields, Gravitation, and Cosmology*, 76(6):064004, 2007.
- [34] Indira Ocampo, George Alestas, Savvas Nesseris, and Domenico Sapone. Enhancing cosmological model selection with interpretable machine learning. *arXiv preprint arXiv:2406.08351*, 2024.
- [35] Jens Chluba, Jan Hamann, and Subodh P. Patil. Features and new physical scales in primordial observables: Theory and observation. *International Journal of Modern Physics D*, 24(10):1530023, June 2015.
- [36] Shadab Alam, Metin Ata, Stephen Bailey, Florian Beutler, Dmitry Bizyaev, Jonathan A Blazek, Adam S Bolton, Joel R Brownstein, Angela Burden, Chia-Hsun Chuang, et al. The clustering of galaxies in the completed sdss-iii baryon oscillation spectroscopic survey: cosmological analysis of the dr12 galaxy sample. *Monthly Notices of the Royal Astronomical Society*, 470(3):2617–2652, 2017.
- [37] Timothy MC Abbott, Michel Aguena, Alex Alarcon, S Allam, O Alves, A Amon, F Andrade-Oliveira, James Annis, S Avila, D Bacon, et al. Dark energy survey year 3 results: Cosmological constraints from galaxy clustering and weak lensing. *Physical Review D*, 105(2):023520, 2022.
- [38] Jelte TA de Jong, Gijs A Verdoes Kleijn, Konrad H Kuijken, Edwin A Valentijn, KiDS, and Astro-WISE Consortiums. The kilo-degree survey. *Experimental Astronomy*, 35:25–44, 2013.
- [39] Simone Aiola, Erminia Calabrese, Loïc Maurin, Sigurd Naess, Benjamin L Schmitt, Maximilian H Abitbol, Graeme E Addison, Peter AR Ade, David Alonso, Mandana Amiri, et al. The atacama cosmology telescope: Dr4 maps and cosmological parameters. *Journal of Cosmology and Astroparticle Physics*, 2020(12):047, 2020.
- [40] Alain Blanchard, S Camera, Carmelita Carbone, VF Cardone, S Casas, Sébastien Clesse, S Ilić, M Kilbinger, T Kitching, Martin Kunz, et al. Euclid preparation-vii. forecast validation for euclid cosmological probes. *Astronomy & Astrophysics*, 642:A191, 2020.
- [41] Rene Laureijs, Jérôme Amiaux, S Arduini, J-L Augueres, J Brinchmann, R Cole, M Cropper, C Dabin, L Duvet, A Ealet, et al. Euclid definition study report. *arXiv preprint arXiv:1110.3193*, 2011.
- [42] Y Mellier, JA Barroso, A Achúcarro, J Adamek, R Adam, GE Addison, N Aghanim, M Aguena, V Ajani, Y Akrami, et al. Euclid. i. overview of the euclid mission. *arXiv preprint arXiv:2405.13491*, 2024.
- [43] Željko Ivezić, Steven M Kahn, J Anthony Tyson, Bob Abel, Emily Acosta, Robyn Allsman, David Alonso, Yusra AlSayyad, Scott F Anderson, John Andrew, et al. Lsst: from science drivers to reference design and anticipated data products. *The Astrophysical Journal*, 873(2):111, 2019.
- [44] Behzad Abareshi, J Aguilar, S Ahlen, Shadab Alam, David M Alexander, R Alfarsy, L Allen, C Allende Prieto, O Alves, J Ameel, et al. Overview of the instrumentation for the dark energy spectroscopic instrument. *The Astronomical Journal*, 164(5):207, 2022.

- [45] Rémy Joseph, Peter Melchior, and Fred Moolekamp. Joint survey processing: combined resampling and convolution for galaxy modelling and deblending. *arXiv preprint arXiv:2107.06984*, 2021.
- [46] Cora Dvorkin, Siddharth Mishra-Sharma, Brian Nord, V Ashley Villar, Camille Avestruz, Keith Bechtol, Aleksandra Ćiprijanović, Andrew J Connolly, Lehman H Garrison, Gautham Narayan, et al. Machine learning and cosmology. *arXiv preprint arXiv:2203.08056*, 2022.
- [47] Kana Moriwaki, Takahiro Nishimichi, and Naoki Yoshida. Machine learning for observational cosmology. *Reports on Progress in Physics*, 86(7):076901, 2023.
- [48] Jonah C Rose, Paul Torrey, Francisco Villaescusa-Navarro, Mariangela Lisanti, Tri Nguyen, Sandip Roy, Kassidy E Kollmann, Mark Vogelsberger, Francis-Yan Cyr-Racine, Mikhail V Medvedev, et al. Introducing the dreams project: Dark matter and astrophysics with machine learning and simulations. *arXiv preprint arXiv:2405.00766*, 2024.
- [49] Koya Murakami, Indira Ocampo, Savvas Nesseris, Atsushi J Nishizawa, and Sachiko Kuroyanagi. Non-linearity-free prediction of the growth-rate $f\sigma_8$ using convolutional neural networks. *arXiv preprint arXiv:2305.12812*, 2023.
- [50] Zhiwei Min, Xu Xiao, Jiacheng Ding, Liang Xiao, Jie Jiang, Donglin Wu, Qiufan Lin, Yin Li, Yang Wang, Shuai Liu, et al. Deep learning for cosmological parameter inference from dark matter halo density field. *arXiv preprint arXiv:2404.09483*, 2024.
- [51] Jorge Enrique García-Farieta, Héctor J Hortúa, and Francisco-Shu Kitaura. Bayesian deep learning for cosmic volumes with modified gravity. *Astronomy & Astrophysics*, 684:A100, 2024.
- [52] Austin Peel, Florian Lalande, Jean-Luc Starck, Valeria Pettorino, Julian Merten, Carlo Giocoli, Massimo Meneghetti, and Marco Baldi. Distinguishing standard and modified gravity cosmologies with machine learning. *Physical Review D*, 100(2):023508, 2019.
- [53] Ye-Peng Yan, Guo-Jian Wang, Si-Yu Li, Yang-Jie Yan, and Jun-Qing Xia. Lensing reconstruction from the cosmic microwave background polarization with machine learning. *The Astrophysical Journal*, 952(1):15, 2023.
- [54] Mehmet Salti and Evrim Ersin Kangal. Deep learning of cmb radiation temperature. *Annals of Physics*, 439:168799, 2022.
- [55] Daniel Baumann. Tasi lectures on primordial cosmology. *arXiv preprint arXiv:1807.03098*, 2018.
- [56] Carolyn Judith MacTavish. *CMB angular power spectra and cosmological implications from the 2003 LDB flight of the BOOMERANG telescope*. University of Toronto, 2006.
- [57] Antony Lewis, Anthony Challinor, and Anthony Lasenby. Efficient computation of cosmic microwave background anisotropies in closed friedmann-robertson-walker models. *The Astrophysical Journal*, 538(2):473–476, 2000.
- [58] Julien Lesgourgues. The Cosmic Linear Anisotropy Solving System (CLASS) I: Overview. *arXiv e-prints*, page arXiv:1104.2932, April 2011.
- [59] Raphaël Kou, Calum Murray, and James G Bartlett. Constraining $f(r)$ gravity with cross-correlation of galaxies and cosmic microwave background lensing. *Astronomy & Astrophysics*, 686:A193, 2024.
- [60] Shinji Tsujikawa. Matter density perturbations and effective gravitational constant in modified gravity models of dark energy. *Physical Review D—Particles, Fields, Gravitation, and Cosmology*, 76(2):023514, 2007.
- [61] Hayato Motohashi, Alexei A Starobinsky, and Jun’ichi Yokoyama. $f(r)$ gravity and its cosmological implications. *International Journal of Modern Physics D*, 20(08):1347–1355, 2011.

- [62] Yong-Seon Song, Wayne Hu, and Ignacy Sawicki. Large scale structure of $f(r)$ gravity. *Physical Review D—Particles, Fields, Gravitation, and Cosmology*, 75(4):044004, 2007.
- [63] Kumar Ravi, Anirban Chatterjee, Biswajit Jana, and Abhijit Bandyopadhyay. Investigating the accelerated expansion of the universe through updated constraints on viable $f(r)$ models within the metric formalism. *Monthly Notices of the Royal Astronomical Society*, 527(3):7626–7651, 2024.
- [64] Suresh Kumar, Rafael C Nunes, Supriya Pan, and Priya Yadav. New late-time constraints on $f(r)$ gravity. *Physics of the Dark Universe*, 42:101281, 2023.
- [65] Deng Wang. Pantheon+ constraints on dark energy and modified gravity: An evidence of dynamical dark energy. *Physical Review D*, 106(6):063515, 2022.
- [66] Kushal Lodha, Lucas Pinol, Savvas Nesseris, Arman Shafieloo, Wuhyun Sohn, and Matteo Fasiello. Searching for local features in primordial power spectrum using genetic algorithms. *arXiv preprint arXiv:2308.04940*, 2023.
- [67] Ahana Kamerkar, Savvas Nesseris, and Lucas Pinol. Machine learning cosmic inflation. *Physical Review D*, 108(4):043509, 2023.
- [68] M Ballardini, Y Akrami, F Finelli, D Karagiannis, Baojiu Li, Y Li, Z Sakr, D Sapone, A Achúcarro, M Baldi, et al. Euclid: The search for primordial features. *Astronomy & Astrophysics*, 683:A220, 2024.
- [69] Jürgen Schmidhuber. Deep learning in neural networks: An overview. *Neural networks*, 61:85–117, 2015.
- [70] Ziad Sakr and Matteo Martinelli. Cosmological constraints on sub-horizon scales modified gravity theories with mgclass ii. *Journal of Cosmology and Astroparticle Physics*, 2022(05):030, 2022.
- [71] SGOPAL Patro and Kishore Kumar Sahu. Normalization: A preprocessing stage. *arXiv preprint arXiv:1503.06462*, 2015.
- [72] Abien Fred Agarap. Deep learning using rectified linear units (relu). *arXiv preprint arXiv:1803.08375*, 2018.
- [73] Nitish Srivastava, Geoffrey Hinton, Alex Krizhevsky, Ilya Sutskever, and Ruslan Salakhutdinov. Dropout: a simple way to prevent neural networks from overfitting. *The journal of machine learning research*, 15(1):1929–1958, 2014.
- [74] Santiago Casas, VF Cardone, Domenico Sapone, N Frusciante, Francesco Pace, Gabriele Parimbelli, M Archidiacono, K Koyama, Isaac Tutusaus, Stefano Camera, et al. Euclid: Constraints on $f(r)$ cosmologies from the spectroscopic and photometric primary probes. *arXiv preprint arXiv:2306.11053*, 2023.
- [75] E Bellini, A Barreira, N Frusciante, B Hu, S Peirone, M Raveri, Miguel Zumalacarregui, A Avilez-Lopez, M Ballardini, RA Battye, et al. Comparison of einstein-boltzmann solvers for testing general relativity. *Physical Review D*, 97(2):023520, 2018.
- [76] Yu Zhang, Peter Tiño, Aleš Leonardis, and Ke Tang. A survey on neural network interpretability. *IEEE Transactions on Emerging Topics in Computational Intelligence*, 5(5):726–742, 2021.
- [77] Scott M Lundberg, Gabriel Erion, Hugh Chen, Alex DeGrave, Jordan M Prutkin, Bala Nair, Ronit Katz, Jonathan Himmelfarb, Nisha Bansal, and Su-In Lee. From local explanations to global understanding with explainable ai for trees. *Nature machine intelligence*, 2(1):56–67, 2020.
- [78] Mukund Sundararajan and Amir Najmi. The many shapley values for model explanation. In *International conference on machine learning*, pages 9269–9278. PMLR, 2020.

- [79] Amirata Ghorbani and James Zou. Data shapley: Equitable valuation of data for machine learning. In *International conference on machine learning*, pages 2242–2251. PMLR, 2019.
- [80] Luis Fernando Machado Poletti Valle, Camille Avestruz, David J. Barnes, Arya Farahi, Erwin T. Lau, and Daisuke Nagai. shaping the gas: understanding gas shapes in dark matter haloes with interpretable machine learning. *Mon. Not. Roy. Astron. Soc.*, 507(1):1468–1484, 2021.
- [81] S. Gilda, S. Lower, and D. Narayanan. mirkwood: Fast and Accurate SED Modeling Using Machine Learning. In *American Astronomical Society Meeting Abstracts*, volume 237 of *American Astronomical Society Meeting Abstracts*, page 215.07D, January 2021.